Dynamic light scattering and viscosity measurements in a ternary and quaternary discotic lyotropic nematic liquid crystal: Tuning the backflow with salt

C. L. S. Risi* and A. M. Figueiredo Neto
Instituto de Física, Universidade de São Paulo, Caixa Postal 66318, 05314-970 São Paulo, São Paulo, Brazil

E. Akpinar
Department of Chemistry, Arts and Sciences Faculty, Abant Izzet Baysal University, 14280 Bolu, Turkey

M. B. Lacerda Santos
Instituto de Física, Universidade de Brasília, 70919-970 Brasília, Distrito Federal, Brazil
(Received 20 April 2013; revised manuscript received 5 July 2013; published 26 August 2013)

Using a dynamic light scattering technique, we measure the damping rate of thermal fluctuations of the nematic director for the so-called disklike nematic N_D phase of both the ternary lyotropic K-laurate–1-decanol–H_2O system and the quaternary one of similar composition except for the addition of salt (K_2SO_4). By varying the scattering angle in suitable geometries and polarizations, we are able to measure the orientational diffusivities associated with the pure deformations of splay and twist. A previous study made in the N_D phase of the same ternary system yielded a large deviation between the splay and twist diffusivities. The effect was then interpreted in terms of the anisotropy between their associated viscosities due to induced flows, or backflow. In the present work we observe a strong increase of the backflow as an effect of the added salt. In addition, we make auxiliary measurements of shear viscosity and magnetic instabilities, which help to characterize the effect of the salt in the orientational diffusivities as they are mixed quantities involving elastic constants and viscosity coefficients.

DOI: 10.1103/PhysRevE.88.022506 PACS number(s): 61.30.Cz, 61.30.Eb, 78.35.+c, 61.30.St

I. INTRODUCTION

Depending on the nature of its basic units, liquid crystals (LCs) are divided into two main classes, namely, thermotropic and lyotropic LCs [1,2]. Classical thermotropic LCs are made of elongated molecules, widely known from industrial applications such as LC displays. In contrast, lyotropic LCs [3] are mixtures of amphiphilic molecules and a solvent, usually water. In moderate concentrations, aqueous solutions of amphiphilic molecules tend to form micelles, which may give rise to nematic phases. All three theoretically predicted types of nematic phases [4] have been found in lyotropic systems. The two uniaxial nematic phases are the discotic N_D and the calamitic N_C [5] phases and the third one is the biaxial N_B phase. The N_B phase has been found in the ternary system consisting of K-laurate, 1-decanol, and water [6] as an intermediate phase between the uniaxial ones. Incidentally, further structural studies [3] seem to favor the so-called intrinsic biaxial micelle (IBM) model, which proposes that the three kinds of lyotropic nematic phases would be different long-range orientational arrangements of micelles of basically the same orthorhombic symmetry.

It is known that some of the main physical properties of lyotropic and thermotropic nematic liquid crystals are quite similar. In particular, the orders of magnitude of the elastic constants for lyotropic and thermotropic nematics are the same [1,3]. Besides, for most nematic LCs, elastic constants show a relatively weak anisotropy, regardless of the class they belong to.

Thermal fluctuations of the orientational director are at the origin of the strong scattering of light observed in nematic liquid crystals. Assuming a uniaxial nematic phase, let us denote its optical axis by the unit vector $\mathbf{n}_o$, which specifies the average direction of alignment. Following de Gennes, the fluctuations of the local director $\mathbf{n}$ may be decomposed into two normal modes [7], defined in terms of the plane $(\mathbf{n}_o,\mathbf{q})$, where $\mathbf{q}$ is a wave vector associated with a Fourier component of the fluctuations. Thus the normal modes δn_1 and δn_2 are respectively parallel and perpendicular to the plane $(\mathbf{n}_o,\mathbf{q})$, that is (see Fig. 1 of [8]),

$$\mathbf{n} = \mathbf{n}_o + \delta n_1 \mathbf{e}_1 + \delta n_2 \mathbf{e}_2. \tag{1}$$

Here δn_1 and δn_2 are modes made of a combination of splay and bend deformations and twist and bend deformations, respectively. The relaxation rates Γ of the director fluctuations were initially measured [9] by light beating or photon correlation techniques, yielding information about elastic and viscous properties of LC systems. For a nematic phase, Γ_i is given by

$$\Gamma_i = \frac{1}{\eta_i(\mathbf{q})}(K_i q_\perp^2 + K_3 q_\parallel^2), \tag{2}$$

where $i = 1,2$ refer to the above-defined fluctuation modes, $q_\parallel$ and $q_\perp$ are respectively the components of the scattering wave vector $\mathbf{q}$ parallel and normal to the optical axis $\mathbf{n}_o$. Finally, K_1, K_2, and K_3 are the Frank elastic constants for splay, twist, and bend deformations, respectively.

Symmetric scattering geometries may lead to simpler formulas. As an example, for $\mathbf{q} \perp \mathbf{n}_o$ (see Fig. 1), depolarized scattering provides information about pure deformations of twist, giving

$$\Gamma_{\text{twist}} = \frac{K_2}{\eta_{\text{twist}}} q^2 \equiv D_{\text{twist}} q^2, \tag{3}$$

*celsorisi@usp.br

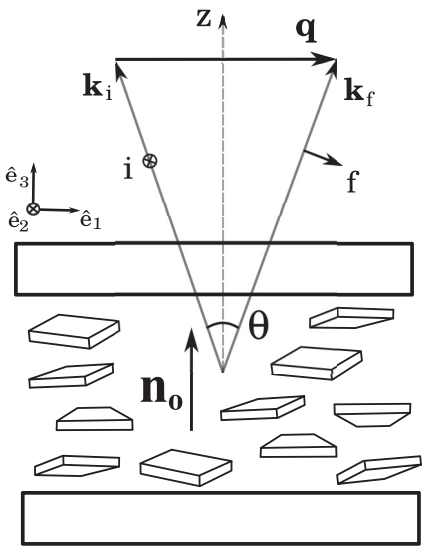

FIG. 1. Symmetric-scattering geometry around the nematic director. In homeotropic alignment, ordinary-extraordinary polarization yields detection of the pure twist fluctuations. Schematic view of the N_D phase, according to the intrinsically biaxial micelle model [3].

where $\eta_{\text{twist}} \equiv \gamma_1$ is the rotational viscosity coefficient [10] and q is related to the (internal) scattering angle θ according to $q = 2k_L n \sin(\theta/2)$, where $k_L = 2\pi/\lambda$ is the laser wave vector and n is the mean refractive index of the medium. Indeed, by a certain choice of geometries and polarizations, photon correlation measurements allow determination of the so-called diffusivities D_{splay}, D_{twist}, and D_{bend} given by relationships analogous to Eq. (3), that is, an elastic constant divided by a viscosity coefficient.

Rayleigh scattering, or more specifically dynamic light scattering (DLS), experiments have been performed on both thermotropic [9] and lyotropic [11,12] uniaxial nematics, yielding measurements of orientational diffusivities. By probing two different geometries, a large deviation between the corresponding diffusivities may be found. Whenever it occurs, such a large anisotropy could hardly be attributed to elastic constants. Therefore, we can focus our attention on the viscosity coefficients only. For classical thermotropic nematics, it is well known that one usually has $\eta_{\text{bend}} \ll \gamma_1$. This result can be explained in terms of the nematodynamic equations thanks to a backflow effect [1,13], which means that induced flows assist the bend fluctuations of the elongated rods, reducing the internal dissipation. In principle, the splay fluctuations would also benefit from a reduction on its associated friction coefficient, but the weak coupling with the flow parallel to $\mathbf{n}_o$ actually makes such a reduction negligible.

The latter appearance of lyotropic nematics brought new elements to the matter. As seen above, they present not a single but two types of uniaxial nematic phases. Light scattering measurements in the N_D phase yielded [11] $D_{\text{splay}} \sim 7D_{\text{twist}}$. Such a large deviation cannot be explained by the usually modest anisotropy between the elastic constants K_1 and K_2. (If K_3 were involved, a larger deviation, of a factor of 2 or 3, could be expected, but it is still not enough to explain the quoted anisotropy on the diffusivities.) Thus this clearly indicates that $\eta_{\text{splay}} \ll \gamma_1$. Therefore, regarding the backflow effect, the lyotropic discotic nematic shows a reversed behavior compared to the classical thermotropic nematic made of rodlike molecules as well as to the lyotropic calamitic nematic [8].

This reversal between splay and bend was explained by the authors of Ref. [11] in terms of the interchange of the role played by the basic units of the phases (assumed to be disks and cylinders) in each of the two uniaxial nematic phases. That is, splay in N_D looks like bend in N_C (see Fig. 3 of Ref. [8]). For further discussion see also Ref. [14].

Though being a rather old subject, Rayleigh scattering of liquid crystals remains a potentially vast field but still lacks basic knowledge in its scarce literature. For instance, very few papers present data allowing us to separate the effect of viscosities and elastic constants in the measured diffusivities. As a step in this direction, in the present paper we report combined DLS and (shear) viscosity measurements of the N_D phase of two kinds of lyotropic mixtures, namely, ternary and quaternary ones. The latter was recently prepared in our laboratory [15,16] and features the addition of a salt on the classical ternary system mentioned above. Although the strong effect of adding salt to lyotropic mixtures has been known for a long time regarding structural properties [3], much less is known about the influence of salt on the dynamic behavior of these materials. Our results show that salt influences both DLS and viscosity measurements, which opens possibilities of controlling the properties of lyotropic liquid crystals.

The paper is organized in as follows. Section II is devoted to the experimental aspects of the samples and techniques employed. Section III discusses the background of DLS theory. The results and a discussion are presented in Sec. IV. Section V provides a summary.

II. EXPERIMENT

A. Sample preparation for light scattering experiments

Regarding light scattering and viscosity measurements, four lyotropic liquid crystal samples were prepared, all of them presenting the N_D phase through a temperature interval of several °C to approximately 20 °C. One sample is of the classical ternary mixture already mentioned [6,17] of potassium laurate (KL), 1-decanol, and H_2O, with a composition of 27.0, 7.4, and 65.6 wt.%, respectively (or 2.98, 1.23, and 95.79 mol%), hereafter called Nd3. This mixture exhibits a phase sequence, as a function of the temperature: $N_D \leftrightarrow N_B \leftrightarrow N_C$ at 22 °C and 27 °C, respectively. The N_D phase was observed until (decreasing) temperatures of about 15 °C. The phases and phase transitions were determined by use of convergent laser light (conoscopy) [5] and optical microscopy observations. The remaining samples are different quaternary mixtures [16], namely, the KL–K_2SO_4–1-decanol–H_2O mixture. Notice here two features: first the presence of salt (potassium sulfate) and second that we have kept the same cosurfactant 1-decanol of the classical mixture in the particular quaternary system chosen. The three quaternary samples, hereafter called Nd4a, Nd4b, and Nd4c, have increasing salt concentrations of 1.6, 2.4, and 3.2 wt.% or, equivalently, 0.25, 0.38, and 0.51 mol%. The full compositions of the four samples are displayed in Table I. Next we discuss additional auxiliary samples that we have prepared for elastic constant determinations.

TABLE I. Composition (in mol%) of the different nematic mixtures investigated.

	Composition (mol%)			
Sample	K-laurate	K_2SO_4	1-decanol	water
Nd3	2.98		1.23	95.79
Nd4a	3.23	0.25	1.22	95.30
Nd4b	3.23	0.38	1.21	95.18
Nd4c	3.22	0.51	1.22	95.05

B. Determination of the ratio K_3/χ_a

In this section the experimental details of the K_3/χ_a determination are described. We employed the method proposed by Kroin and Figueiredo Neto [18] to measure this ratio in nematic calamitic N_C phases. In spite of our main concern in this paper with the N_D phase, we expect that these auxiliary measurements allow us to gain some knowledge of how the elastic constant (in the spirit of the one-constant approximation [1]) behaves as salt is added into the lyotropic mixture.

Three lyotropic mixtures were prepared for this investigation, one ternary and two quaternary. The ternary mixture (Nc3) is composed of K-laurate, 1-decanol, and water (28.7, 7.2, and 64.1 wt.%, or 3.23, 1.22, and 95.55 mol%), with the phase sequence as a function of the temperature starting from the isotropic I phase, $I \leftrightarrow N_C \leftrightarrow I$ at 15 °C and 47 °C, respectively. The two quaternary mixtures Nc4a and Nc4b are composed of K-laurate, K_2SO_4, 1-decanol, and water, 28.6, 0.5, 7.2, and 63.7 wt.% (or 3.24, 0.077, 1.23, and 95.46 mol%) and 28.5, 1.0, 7.1, and 63.4 wt.% (or 3.24, 0.16, 1.22, and 95.39 mol%), respectively. These stoichiometries were chosen so that the mixtures presented the N_C phase at 20 °C. Flat glass microslide cells (20 mm long, 2.5 mm wide, and 200 μm thick) were used in these experiments. The ends of the microslides were sealed with a photoreactive epoxy resin. After this process the samples were subjected to a magnetic field ($H \approx$ 6.5 kG) positioned along the length of the cell for 6 h. In this condition the nematic director orients parallel to **H**. A polarized light microscope was used to check the sample alignment. After complete sample alignment is achieved, the microslides were positioned so that an angle of 90° was formed between the previous aligned director and the external magnetic field. In this condition the nematic director is normal to **H** and tends to reorient to the parallel alignment. This experimental procedure leads to the formation of a texture with periodic inversion walls, which depends on the field strength. The periodicity of the walls P was measured in a cross-polarized microscope. Several amplitudes of **H** were used, from 4.0 to 6.4 kG. From the data of the periodicity lengths as a function of the magnetic field strength we were able to calculate the ratio K_3/χ_a for each sample. Finally, as the literature lacks data about the effect of salt on the diamagnetic anisotropy of the micelles, we assume such an effect as negligible, at the expense of an additional error introduced in our semiquantitative estimates. Adopting $\chi_a \sim 3 \times 10^{-9}$ cgs (a typical value for lyotropic LCs [18]), this allows us to determine K_3 for each sample.

C. Light scattering cell and sample alignment

For light scattering experiments, samples were placed into a rectangular Hellma cuvette, with a 1-mm-thick optical path. The cuvette was cleaned in an ultrasonic bath, using successively acetone, ethyl alcohol, and distilled water. The cuvette stayed in each bath for 30 min. A final bath used warm distilled water (at 70 °C), which allowed efficient drying by simple evaporation. Before the scattering experiments, the LC cell was placed in a magnetic field (7 kG) for 8 h. The homeotropic alignment was achieved by positioning the largest wall planes of the cuvette parallel to the magnetic field. Due to the negative magnetic susceptibility anisotropy of the N_D phase, the nematic director orients perpendicular to the field. In order to break the degeneracy we used a device that periodically rotates the sample holder of an angle of 90°, back and forth, around an axis perpendicular to the magnetic field. With this procedure, the nematic director orients parallel to this rotation axis, perpendicular to the magnetic field. The perfect orientation of the sample was checked by optical microscopy and conoscopic fringe inspection. Only when the sample presented a perfect homeotropic alignment was it used in the DLS measurements.

D. Light scattering setup

Once the alignment process was finished, the sample was positioned on the goniometer in the DLS setup. Figure 2 shows a sketch of the setup. The light source was a low-noise diode-pumped continuous laser from Coherent, model Verdi V6, with a 532-nm wavelength. The range of output power used in the DLS experiments was from 1 to 2 W. The maximum and minimal values of the scattering-vector modulus $|\mathbf{q}|$ achieved in our measurements were, in units of 10^6 m^{-1}, $|\mathbf{q}_{\max}| = 13.3$ and $|\mathbf{q}_{\min}| = 2.0$. In the measurement with the higher q it was necessary to increase the output laser power in order to improve the photon-count statistics.

The laser beam passed through a spatial filter (SF), yielding a clean output beam of Gaussian profile, with a diameter of around 1 mm. The SF device blocked much of the light; only about 15% crossed through the SF.

At the sample position the incident beam had a power of about 1–3 mW, depending on the incident angle. There was no relevant thermal effect in this condition. The filtered beam was then linearly polarized by polarizer P1 (Newport, model No. 10LP-VIS-B) and focused into the sample.

The light scattered by the sample (at a chosen angle θ_{ext}) passes through a pinhole with a diameter smaller than the typical ones of the light spots on the region where light

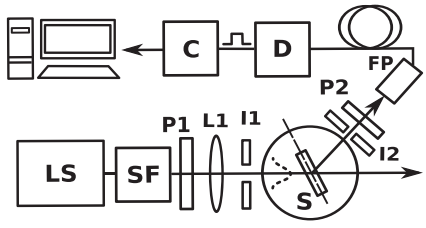

FIG. 2. Dynamic light scattering setup: LS, laser; SF, spatial filter; P1 and P2, polarizers; I1 and I2, irises; S, sample; FP, fiber positioner; D, detector; and C, correlator.

is collected. This coherent area condition is important to ensure a good optical beating signal [19]. Then the scattered light passed through an analyzer (P2) to define the final polarization **f** and was collected by a monomode optical fiber placed in the fiber positioner (FP). The fiber was coupled to the photomultipliers (D), which transmit the signals to the correlator (C), from Correlator Inc. The correlator calculates in real time the normalized autocorrelation function $g_2(\vec{q},\tau)$, where τ is the delay correlation time (discussed further in the following). The lowest value of τ reached by our correlator was 1.56 ns. The acquisition time of the correlation experiments was about 10 min with a typical sample time of about 250 ms.

All measurements were done at room temperature, 20.0 °C (±0.3 °C). This temperature is far enough from phase transitions to avoid significant contribution from pretransitional fluctuations [20] to the scattering signal.

In order to implement the scattering geometry of Fig. 1, suppose that the incident laser beam, along $\mathbf{k}_i$, traverses the sample cell making an (internal) angle of $\theta/2$ with respect to the glass windows normal (z axis). The selection of the scattered wave vector $\mathbf{k}_f$ direction follows an optical alignment procedure that uses the reflected beam from the cell, yielding the symmetrical geometry of Fig. 1 as well as enabling a precise definition of the (horizontal) scattering plane $(\hat{e}_2,\hat{e}_3)$. As $|\mathbf{k}_i| \approx |\mathbf{k}_f|\,(\equiv|\mathbf{k}|)$, due to the low birefringence of lyotropic nematics ($\Delta n \sim 10^{-3}$), this results in $\mathbf{q}$ perpendicular to the z axis. In order to calculate $|\mathbf{k}|$ inside the LC medium we use a (mean) refractive index of $n = 1.38$, which is determined for a lyotropic mixture of neighboring concentrations [11].

Finally, for depolarized DLS measurements we used the incident laser beam vertically polarized, yielding an ordinary incoming polarization, as indicated in Fig. 1. For polarized scattering, in contrast, we used the incident laser beam horizontally polarized, yielding an extraordinary incoming polarization.

E. Viscosity

The shear viscosity of the mixtures was measured by using a viscometer Anton Paar, model SVM 3000. Samples were injected in a tube that rotates at a constant angular velocity. In the tube there was a hollow lightweight rotor, located in the center of the tube, that rotates during the measurement. The rotor reaches a constant angular velocity, which is monitored by a Hall-effect sensor.

The sample temperature was controlled by a Peltier thermostat, with a stability of 0.005 °C. All the measurements were performed at 20 °C. A cleaning protocol was followed before each experiment. First, the cylindrical sample holder was heated up to 60 °C. Then the tube was filled with ethyl alcohol and the viscometer was turned on. An air pump was used to remove the alcohol from the tube. This procedure was repeated five times. After the evaporation of the alcohol, the temperature was set to 20 °C and, after thermal stabilization, the tube was filled with the lyotropic mixture.

III. DYNAMIC LIGHT SCATTERING THEORY

A. Autocorrelation functions

Beyond the structure $S(\vec{q})$ and form factors $F(\vec{q})$, which bear static information, the autocorrelation functions provide dynamic information about the sample, as they are sensitive to thermal fluctuations of the dielectric tensor of the scattering medium [19]. Such fluctuations in turn can originate from fluctuations in local properties such as density and concentration. In the case of a nematic LC, fluctuations of the nematic director are a major source of light scattering [1]. Theoretically, the simplest quantity that provides information about temporal fluctuations of a linearly polarized optical field $\mathbf{E}(\vec{q},t)\cdot\mathbf{f}$ [$\equiv E(t)$, for short] is the (normalized) first-order autocorrelation function $g_1(\vec{q},t)$, which we write for simplicity as [19]

$$g_1(\vec{q},\tau) = \frac{\langle E^*(\vec{q},t)E(\vec{q},t+\tau)\rangle}{\langle|E|^2\rangle}, \tag{4}$$

where the angular brackets stand primarily for time average, but are equivalent to the thermal average in the case of ergodic systems, and $|E|^2$ is to be identified with the instantaneous light intensity $I(\vec{q},t)$.

However, by the nature of the detection process, one does not have direct access to this amplitude correlation function. Instead, one can measure the intensity (second-order) correlation function, which is defined by the normalized function [19]

$$g_2(\vec{q},\tau) = \frac{\langle I(\vec{q},t)I(\vec{q},t+\tau)\rangle}{\langle I(\vec{q},t)\rangle^2}, \tag{5}$$

where $I(\vec{q},t)$ and $I(\vec{q},t+\tau)$ are the light intensities scattered by the sample at a time t and $t+\tau$, respectively, for a given wave vector $\vec{q}$. Here an important simplification arises whenever the optical field is a superposition of contributions from different subregions of the scattering volume that are independent of each other. In such a condition (a so-called Gaussian random process), the random variable has a Gaussian distribution and it can be shown [19] that g_1 and g_2 are linked by the Siegert relationship $g_2(\tau) = 1 + |g_1(\tau)|^2$.

B. Detection regimes

In a homodyne regime, that is, a physical situation in which a pure dynamic optical field signal $E_S(t)$ (which carries information about the hydrodynamic behavior of the sample) beats with itself, one has direct access to $g_2(\vec{q},\tau)$. In contrast, in a heterodyne regime, there is a coherent beating between static and dynamic electric fields at the detector level. This static component, the so-called local oscillator [19] $E_{\mathrm{LO}}(t)$, may result from a variety of sources such as stray light, dust, or, in the case of LC, microdefects.

Concerning the temporal dependence of our correlation functions, notice that in an overdamped scenario, as in the case of nematic LCs [1], one expects that any fluctuating variable X of interest is governed by a diffusion equation, that is, $\partial\delta X/\partial t = D\nabla^2\delta X$, where δX is a deviation of X from its average value $\langle X\rangle$. For a given Fourier component q, the solution for this equation is $\delta X(t) = \delta X(0)e^{-t/\tau_c}$, where $\tau_c = 1/Dq^2$ is the characteristic relaxation time. Thus it follows that g_1 is proportional to $\langle\delta X(0)\delta X(t)\rangle$ and so $g_1 = A_{\mathrm{het}}e^{-t/\tau_c}$, where A_{het} is the signal amplitude coefficient for heterodyne detection, as it will become clear below [Eq. (7)]. Finally, by using the Siegert relation seen above, one finds that in the pure homodyne case the correlation function $g_2(\tau)$ has an

exponential decay behavior as well, but with a characteristic time $\tau_c/2$:

$$g_2(\mathbf{q},\tau) = 1 + A_{\rm hom} e^{-2t/\tau_c}. \quad (6)$$

Now turning again to the homodyne-heterodyne duality, assume that a portion of static laser light $E_{\rm LO}(t)$ (the local oscillator) interferes with the dynamic signal $E_S(t)$. The resulting optical beating means that one must insert the sum $E_{\rm LO}(t) + E_S(t)$ into the intensity correlation $\langle I(t)I(t+\tau)\rangle$. The result contains 16 terms [19,21], but only the slow time varying terms (and the dc terms) contribute to the time average. One arrives at

$$\langle I(t)I(t+\tau)\rangle = (I_{\rm LO} + I_S)^2 + 2I_{\rm LO}I_S g_1(\tau) + I_S^2|g_1(\tau)|^2, \quad (7)$$

where $I_{\rm LO} = \langle|E_{\rm LO}|^2\rangle$, $I_S = \langle|E_S|^2\rangle$, and we have used the Siegert relation.

Notice that when the local oscillator is much stronger that the signal, i.e., $|E_{\rm LO}| \gg |E_S|$, the homodyne contribution $I_S^2 g_2$ $[=I_S^2 + I_S^2 g_1^2(\tau)]$ can be neglected. Thus, in this case we have a pure heterodyne regime and the autocorrelation function measures directly τ_c.

Of course, the question remains of how to deal with mixed homodyne and heterodyne situations. In the context of an experiment such as ours (that is, Rayleigh scattering in LCs), one might suppose that, at low angles ($\theta < 10^\circ$), the signal tends to be a pure heterodyne one. For higher angles, in contrast, one can expect that some mixture with a homodyne signal may occur, mainly in the case of depolarized light signals, which normally contains much less stray light.

Assuming a single-exponential process, the main difference is that the homodyne contribution has one-half of the characteristic time of the heterodyne one. A two-exponential fit is unable to resolve two components of characteristic times that differ by a factor of 2 between them.

Actually, the criterion to quantify heterodyne and homodyne contributions makes use of the baselines. First, notice that the Siegert relationship suggests a baseline $B = 1$ for a pure homodyne signal, which is essentially due to a dc contribution [19]. (Actually, a shot-noise term has to be added, as it can be seen in the full treatment of the problem, considering the photoelectron statistics [21]. Nevertheless, the shot-noise contribution is easily overlooked, as it affects only the accumulation channels on a very short time scale.) Next, the baseline B for a heterodyne signal can of course be normalized to one, but then one must have $B \gg A_{\rm het}$ because of additional dc contributions from Eq. (7).

Now we discuss how to treat the case of a small homodyne contribution. In order to correct these data (typically within $\sim$10%) we use an approximate method [22] that can be summarized as follows. Let us define the ratio R between the amplitude A of our mixed signal and the baseline B, i.e., $R = A/B$. For a single-exponential process we may set

$$A_{\rm hom} e^{-2t/\tau_c} + A_{\rm het} e^{-t/\tau_c} = A(t) e^{-t/\tau_A}, \quad (8)$$

where

$$A(t) = e^{-(1/\tau_c - 1/\tau_A)t}(A_{\rm het} + A_{\rm hom} e^{-t/\tau_c}). \quad (9)$$

The approximation consists of replacing $A(t)$ by $A(0)$, which can only be valid if $A_{\rm hom} \ll A_{\rm het}$. Hence $A(0) = A_{\rm het} + A_{\rm hom} = 2I_{\rm LO}I_S + I_S^2$, where we used Eq. (7) in the considered approximation. Thus one can deduce the ratio $R = A/B$ as being

$$R = \frac{2I_{\rm LO}I_S + I_S^2}{(I_{\rm LO} + I_S)^2} = 1 - \frac{1}{(1+\alpha)^2}, \quad (10)$$

where $\alpha \equiv I_S/I_{\rm LO}$. The inverse relationship allows us to know α for a given R. Regarding the characteristic times, we know that $R = 0$ (the pure heterodyne case) corresponds to $\tau_A/\tau_c = 1$, while for $R = 1$ (pure homodyne) one has $\tau_A/\tau_c = 0.5$. For the intermediate cases the final step of the method consists of a numerical procedure [22] of simulating the sum of Eq. (8) for different τ_c values and then extracting τ_A through a single-exponential fit. A practical graphic device (Abacus, reproduced in Fig. 4 of Ref. [8]) can be generated, giving directly the correction factor τ_A/τ_c as a function of R.

C. Selection rules

Let us recall the main results of the hydrodynamic theory of light scattering by orientational fluctuations [1,9]. In the so-called polarized geometry (i.e., with both the electric field of the incident beam $E\mathbf{i}$ and the one of the detected scattered beam $E\mathbf{f}$ in the scattering plane), we expect to detect fluctuations of mode 1, namely, a superposition of splay and (in-plane) bend deformations. Now consider the symmetric scattering geometry that we have implemented according to Fig. 1. As seen above, in this arrangement the nematic director lies in the scattering plane defined by $\hat{e}_1$ and $\hat{e}_3$. Moreover, in this geometry the wave vector $\mathbf{q}$ is normal to the nematic director and parallel to $\hat{e}_1$. There is no parallel (to the director) component of the wave vector ($q_{||} \approx 0$). In these conditions, mode 1 is reduced to pure splay fluctuations. However, rigorously speaking, the scattering cross section for mode 1 in this symmetric geometry is zero, according to a selection rule that can be easily deduced from the cross section formula given in Ref. [23], namely,

$$\frac{d\sigma}{d\Omega} = A \sum_{\alpha=1}^{2} \langle|n_\alpha(\mathbf{q})|^2\rangle (i_\alpha f_\parallel + i_\parallel f_\alpha)^2, \quad (11)$$

where $i_\alpha = \mathbf{i}\cdot\hat{e}_\alpha$, $f_\alpha = \mathbf{f}\cdot\hat{e}_\alpha$, and the angular brackets denote thermal average. Nonetheless, as will be seen in Sec. IV, a weak (noisy) but useful polarized signal can be detected, presumably leaky by residual misalignments in our scattering geometry and polarization adjustments.

Now turning to the depolarized configuration, that is (in the ordinary-extraordinary case that we use), the one in which the electric field of the incident beam is perpendicular to the scattering plane and that of the detected scattered beam is in the scattering plane, we obtain mode 2, reduced to pure twist fluctuations because of our symmetric scheme. Now the selection rule is favorable and we obtain a strong twist signal.

D. Relaxation rates

As seen in the Introduction, by particularizing Eq. (2) to our symmetric scattering geometry of Fig. 1 one can expect, for mode 2, pure twist fluctuations detected in the (ordinary-extraordinary) depolarized configuration, with relaxation rates

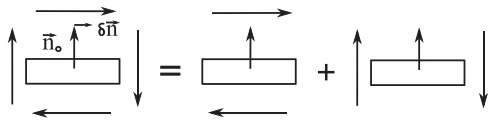

FIG. 3. Sketch of the backflow mechanism.

Γ_{twist}, given by Eq. (3). Similarly, for the (extraordinary-extraordinary) polarized configuration Eq. (2) predicts, for mode 1 in the symmetric geometry, pure splay fluctuations with relaxation rates given by

$$\Gamma_{\text{splay}} = \frac{K_1}{\eta_{\text{splay}}} q^2 \equiv D_{\text{splay}} q^2. \tag{12}$$

E. Backflow

The backflow mechanism has been known for a long time for classical nematics made of rodlike molecules [1,2]. Some particularities applying to disklike objects (eventually, micelles) are discussed in Refs. [11,14]. Here we only summarize the main facts.

Figure 3 illustrates how the flow vortex of a disk rotating with angular velocity ω ($=|d\mathbf{n}/dt|$) can be decomposed into two pure shear flows, one parallel and the other perpendicular to the disk plane. This is important in order to analyze how individual vortices interfere for each of the pure deformations we are dealing with. For instance, in the case of splay ($\mathbf{q} \perp \mathbf{n}_o$) the shear flows parallel to the disks cancel by interference. In contrast, the shear flows perpendicular to the disks interfere constructively to give a macroscopic backflow. (For a better visualization the reader may find it helpful to consider equal phase planes, as in Fig. 3 of Ref. [8].) The backflow tends to suppress relative motions of the micelles. The residual dissipation comes from the local shear parallel to the disk (or plate) plane. The resulting splay viscosity is $\eta_{\text{splay}} \sim \eta$.

In the case of twist, in contrast, there is no backflow, as the interference is totally destructive. (Notice that here too $\mathbf{q} \perp \mathbf{n}_o$, but full vortices belong to any equal phase plane that one wants to consider.) Therefore, twist fluctuations are subject to the full dissipation of a single micelle rotating in the bulk fluid, that is, $\eta_{\text{twist}} \sim \gamma_1$. Moreover, an estimate of γ_1 is made in Ref. [11] (by extending an argument due to Helfrich [24]), namely, $\gamma_1 \sim \eta D^3/a^3$, where a and D are the micelle thickness and diameter, respectively. For our ternary sample (Nd3) available x-ray data [3] give $D \approx 6$ nm and $a \approx 2$ nm, yielding $\gamma_1 \sim 10\eta$.

Finally, in the case of bend, only the friction from shear flows parallel to the plate faces is suppressed by the backflow. The viscosity reduction must be of the order of η compared to γ_1. In other words, we expect that the bend and twist viscosities are comparable.

In terms of the nematodynamic equations, one may summarize this discussion of the compared viscosities of pure twist, splay, and bend deformations in a discotic nematic phase by the relationships

$$\eta_{\text{twist}} = \gamma_1, \quad \eta_{\text{splay}} = \gamma_1 - \frac{(\alpha_3)^2}{\eta_b}, \quad \eta_{\text{bend}} = \gamma_1 - \frac{(\alpha_2)^2}{\eta_c}, \tag{13}$$

where the Leslie α and Miesowicz viscosity coefficients follow the same notations as in Ref. [1]. In the last two expressions the backflow effect is accounted for by the negative terms. An evaluation of these backflow terms in the cases of splay and bend is given in Ref. [11], yielding $\gamma_1 - \eta$ and η, respectively.

IV. RESULTS AND DISCUSSION

A. Determination of the ratio K_3/χ_a

Figure 4 shows the experimental results of bend distortion experiments. Each value of the periodicity length P represents a mean value of ten independent measurements. The error bars are the standard deviations. Our results are consistent with the predicted [18] linear behavior of P^{-2} as a function of H^2:

$$P^{-2} = \left(\frac{1}{4\pi^2}\frac{\chi_a}{K_3}\right) H^2. \tag{14}$$

Linear fits to these data allow us to determine the K_3/χ_a ratio for the different mixtures at the N_C phase. In the case of the Nc3 sample, we find $K_3/\chi_a = 279 \pm 29$ dyn, which is consistent with the value previously obtained in a similar mixture [18]. The quaternary mixtures (Nc4a and Nc4b) show a slight decrease in the K_3/χ_a values: 247 ± 30 and 240 ± 22 dyn, respectively. The experiment shows that there is a slight tendency to decrease the K_3/χ_a values with the addition of salt in the mixture, with respect to the original ternary mixture value. However, with the higher salt concentrations used in the N_D samples the effect (not measured here) could be more pronounced. The anisotropy of diamagnetic susceptibility of the lyotropic mesophase is mainly due to the amphiphilic molecules present in the micelles (i.e., the KL and the alcohol).

The sign of χ_a changes, depending on the particular uniaxial nematic phase N_C or N_D; however, its absolute value lies in the range from about 2×10^{-9} to about 10^{-8} cgs units in different lyotropic mixtures (with main amphiphile KL, phase N_C [25]; sodium decylsulfate, phase N_C [25]; or decylammonium chloride, phase N_D [26,27]). Moreover, assuming that in lyotropic mixtures with two amphiphiles, which present the nematic phases, the IBM model [3] applies and orientational fluctuations of intrinsically orthorhombic micelles give rise to the different nematic phases, it is reasonable to assume that χ_a is approximately constant in all the samples investigated. In this framework, since the value of the ratio K_3/χ_a obtained in

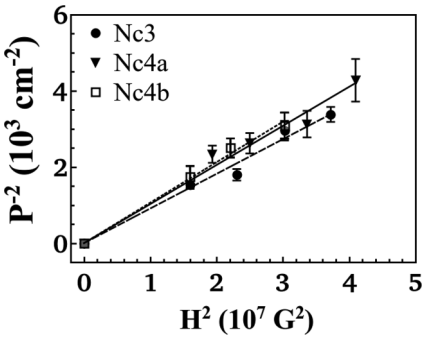

FIG. 4. Plots of the inverse squared field-induced periodicity length as a function of the magnetic field, enabling the determination of K_3/χ_a.

TABLE II. The DLS measurements of the orientational diffusivities D_{splay} ($=K_1/\eta_{\text{splay}}$) and D_{twist} ($=K_2/\gamma_1$) at 20 °C of the discotic nematic samples and the ratio between these diffusivities. The last column shows the shear viscosity measurements η of the same samples at the same temperature. The DLS data quoted from the literature for comparison (row 2) were taken at 19 °C.

Sample	D_{splay} (10^{-12} m^2/s)	D_{twist} (10^{-12} m^2/s)	$\frac{D_{\text{splay}}}{D_{\text{twist}}}$	η (mPa s)
Nd3	9.6 ± 0.2	1.40 ± 0.04	6.9	90.5 ± 0.5
Nd3 [11]	11.5	1.6	7.2	
Nd4a	19.0 ± 0.5	1.25 ± 0.05	15	204 ± 2
Nd4b	55 ± 3	0.18 ± 0.05	305	339 ± 4
Nd4c	44 ± 3	0.11 ± 0.05	400	465 ± 1

our experiment is also approximately constant as a function of the salt concentration, it is reasonable to assume that the value of the elastic constant $K_3 \sim 2 \times 10^{-11}$ N also does not depend on the salt concentration and the particular phase (N_C or N_D). These considerations will be important in the discussion of the DLS experimental results.

B. Viscosity data

As explained in Sec. II, we have measured the shear viscosity of the ternary sample Nd3 and the quaternary ones Nd4a, Nd4b, and Nd4c, at 20 °C. The results are presented in the last column of Table II, as well as in Fig. 8(a). Notice that the shear viscosity increases monotonically as the salt content of the lyotropic mixture increases.

C. Dynamic light scattering

1. Ternary mixture

Figure 5(a) shows the polarized and depolarized autocorrelation signals from the Nd3 mixture. From the respective single-exponential fit [Eq. (6), taking the pure homodyne approximation] we extract the characteristic times τ_c of the twist (≈254 ms) and the splay relaxations (≈35 ms) for $\mathbf{q} = 6.03 \times 10^6 m^{-1} \hat{e}_3$. Such results, with splay fluctuations much faster than twist ones, are consistent with the backflow effect. Figure 5(b) shows the relaxation rates of splay $\Gamma_{\text{splay}} = D_{\text{splay}} q^2$ (high frequencies) and twist $\Gamma_{\text{twist}} = D_{\text{twist}} q^2$ (low frequencies) as a function of q^2. For all graphs like these we have plotted the mean values of the relaxation rates over five measurements taken for each scattering angle, as well as the corresponding standard deviations.

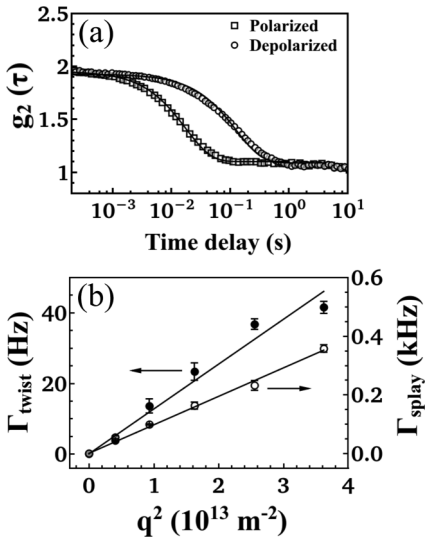

FIG. 5. (a) Splay (polarized) and twist (depolarized) autocorrelation signals measured in the ternary Nd3 sample. The solid lines correspond to single-exponential fits to Eq. (6), with $\mathbf{q} = 6.03 \times 10^6 m^{-1} \hat{e}_3$. (b) Relaxation rates of pure splay (high-frequency) and twist (low-frequency) fluctuations as a function of q^2. Solid lines are linear fits whose slopes determine the orientational diffusivities.

From the linear fits one can extract the diffusivities D_{splay} and D_{twist}, which are shown in Table II. From them one can derive the corresponding splay and twist viscosities, provided the respective elastic constants are known. As this knowledge is scarce in the literature, we assume the one-elastic-constant approximation, i.e., $K_1 \sim K_2 \sim K_3 \sim 2 \times 10^{-11}$ N [25]. The viscosity coefficients resulting from this initial procedure appear in Table III as $\widetilde{\eta}_{\text{splay}}$ and $\widetilde{\eta}_{\text{twist}}$ ($=\widetilde{\gamma}_1$). Our values agree with those previously published for a similar lyotropic mixture [11].

2. Quaternary mixtures

Figure 6 shows typical depolarized [Fig. 6(a)] and polarized [Fig. 6(b)] autocorrelation signals from the three quaternary mixtures. Figure 6(a) refers to the twist fluctuations at $\mathbf{q} = 7.94 \times 10^6 m^{-1} \hat{e}_1$ and Fig. 6(b) to the splay fluctuations at $\mathbf{q} = 4.04 \times 10^6 m^{-1} \hat{e}_1$. The solid lines are fits performed according to Sec. III B using a Levenberg-Marquardt algorithm. From the fits the values of the relaxation rates Γ_{splay} and Γ_{twist} and the respective standard deviations were determined. In order to obtain D_{splay} and D_{twist} we plotted the relaxation rates as a

TABLE III. Viscosities $\widetilde{\gamma}_1$, $\widetilde{\eta}_{\text{splay}}$, and $|\widetilde{\Delta\eta}|$ (backflow) estimated from diffusivity data (at 20 °C) according to the first step of the hypothesis (single K value) and viscosities γ_1, η_{splay}, and $|\Delta\eta|$ (backflow) estimated from diffusivity data (at 20 °C) according to the second step of the hypothesis [$K(\phi)$; see the text].

Sample	K (10^{-11} N)	$\widetilde{\gamma}_1$ (Pa s)	$\widetilde{\eta}_{\text{splay}}$ (Pa s)	$\lvert\widetilde{\Delta\eta}\rvert$ (Pa s)	$K(\phi)$ (10^{-11} N)	γ_1 (Pa s)	$\eta_{\text{splay}} \equiv \eta$ (Pa s)	$\lvert\Delta\eta\rvert$ (Pa s)
Nd3	2	14.3	2.1	12	0.0869	0.621	0.0905	0.531
Nd4a	2	16.0	1.1	15	0.388	3.10	0.204	2.90
Nd4b	2	110	0.4	110	1.86	103	0.339	102.7
Nd4c	2	180	0.5	180	2.05	186	0.465	185.5

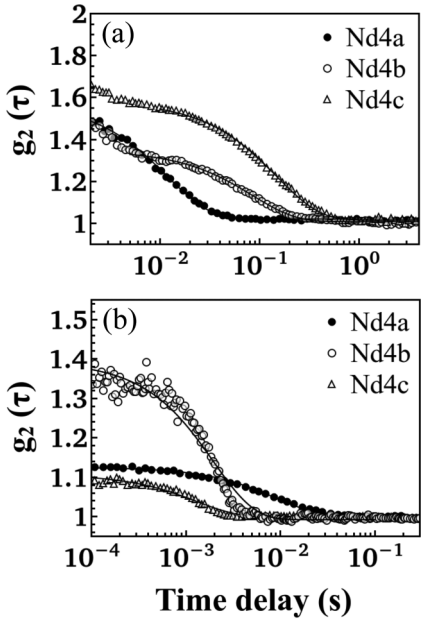

FIG. 6. (a) Typical depolarized autocorrelation signals from the quaternary mixtures leading to the relaxation time of the twist mode at $\mathbf{q} = 7.94 \times 10^6 m^{-1} \hat{e}_1$. (b) Typical polarized autocorrelation signals from the quaternary mixtures with the characteristic signal for the pure splay mode at $\mathbf{q} = 4.04 \times 10^6 m^{-1} \hat{e}_1$. Solid lines are fits from using $g_2(\mathbf{q},\tau) = 1 + A_{\text{het}} e^{-t/\tau_c}$.

function of q^2 (Fig. 7) and performed the corresponding linear fits, as described for the ternary mixture.

Autocorrelation data of Fig. 6(a), all taken at a moderately high angle value $\theta = 28.2^\circ$, have some homodyne character that can be quantified by the parameter R defined in Sec. III B. Thus the curve for the Nd4c sample is the most homodyne among all shown in Fig. 6, with $R \approx 0.6$. By using the graphic device Abacus we obtain a correction factor $\tau_A/\tau_c \approx 0.9$.

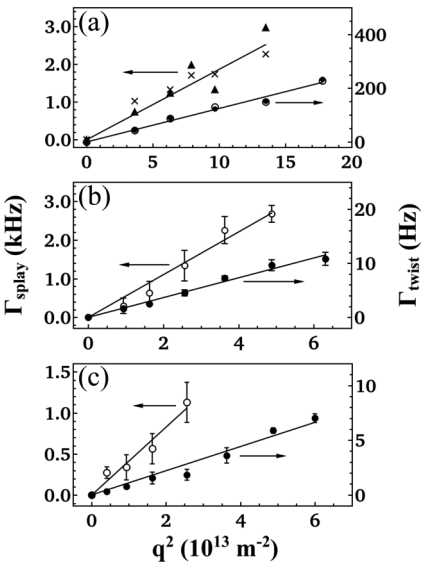

FIG. 7. Relaxation rates of pure splay (high-frequency) and twist (low-frequency) fluctuations as a function of q^2 for the quaternary mixtures (a) Nd4a, (b) Nd4b, and (c) Nd4c. Solid lines are linear fits.

In contrast, the two lowest curves of Fig. 6(b), with $R \approx 0.1$, can be considered as pure heterodyne, within an error of $\sim$1%. The higher curve (sample Nd4b), in contrast, with $R \approx 0.38$, has a surprisingly high homodyne level for a rather low angle value $\theta = 14.2^\circ$. This indeed is to be indebted to a certain trick, which consists of a slight adjustment of the detector optical fiber positioner in order to minimize the local oscillator.

Finally, we mention the presence of a nondiffusive (i.e., q-independent) weak fast signal ($\sim$3 ms), which can arise in either polarized or depolarized light. This signal is not always seen; depending on the wave vector, it may be not detected. A possible interpretation for that signal, in terms of micellar fluctuations, is discussed in Ref. [28]. In this paper we shall not be concerned with it.

However, this fast signal may disturb the measurement of the characteristic time τ_c for slow fluctuations. In such situations we have performed two fits, namely, one with a single exponential, considering the slow signal only, and the other with two exponentials, covering both fast and slow signals. By comparing the two fits we could establish an uncertainty of 12–15 % on the τ_c value under analysis.

Now we analyze the results from the addition of the salt in the originally ternary lyotropic mixture, i.e., sample Nd4a: Our results (Table II) indicate that D_{splay} in the salty mixture is about twice the value of that in the ternary mixture; however, D_{twist} slightly decreases with respect to the value measured in the ternary mixture. Both tendencies are (coarsely) confirmed by analyzing the values of these parameters as a function of the salt concentration, i.e., increasing the salt concentration in the quaternary mixtures, D_{twist} tend to decrease and D_{splay} tend to increase. With respect to D_{splay}, the value obtained with the mixture with the higher salt concentration (Nd4c) showed a small decrease with respect to the former mixture (Nd4b), indicating a possible saturation behavior. The ratio $D_{\text{splay}}/D_{\text{twist}}$ increases with the salt concentration in the sample, a behavior similar to the one of the shear viscosity η (see Table II).

Given the lack of detailed data on elastic constants, we have to adopt hypotheses. We shall do this in two steps. In the first one we assume that the same elastic constant approximation taken for the ternary system applies everywhere, yielding the first-step estimates for $\widetilde{\eta}_{\text{splay}}$ and $\widetilde{\gamma}_1$ (see Table III). We can see that $\widetilde{\gamma}_1$ rises strongly for increasing amounts of salt in the sample [see Fig. 8(c)], a behavior also seen in the shear viscosity measurements.

In contrast, notice that the viscosity $\widetilde{\eta}_{\text{splay}}$ decreases as the salt concentration increases [see Fig. 8(a)] until reaching a value practically equal to the shear viscosity at $\phi = 0.38$ mol %. In this approximation, $D_{\text{splay}}/D_{\text{twist}} \sim \gamma_1/\eta_{\text{splay}}$, increasing with the salt concentration in the sample. The backflow term $\Delta\eta = -\alpha_3^2/\eta_b$ may be calculated from our data as a function of salt concentration, in the one-elastic-constant approximation. The absolute value $|\Delta\eta|$ increases as a function of the salt concentration [see Table III; we omit the graphics of $|\Delta\eta|$ as it looks very nearly like the one of γ_1; see Fig. 8(c)], reaching values about one order of magnitude bigger than that of the ternary mixture (salt-free).

Next, in the second step of the procedure we use the shear viscosity η measurements to improve upon the first step of the approach. As we have seen above, $\widetilde{\eta}_{\text{splay}}$ shows a strong

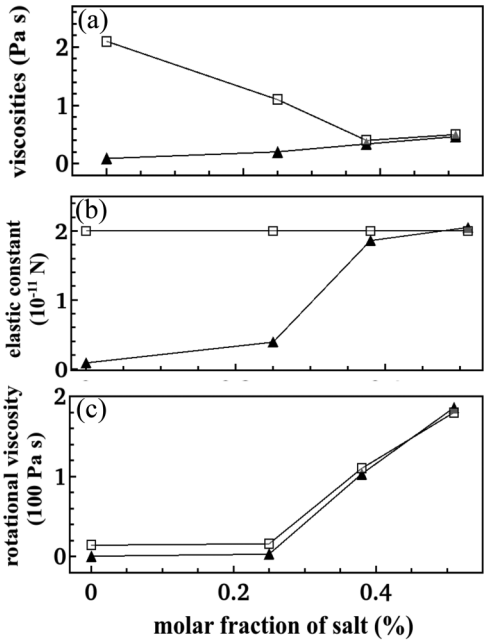

FIG. 8. (a) Squares denote the initial estimates of the splay viscosity $\widetilde{\eta}_{\text{splay}}$ versus the molar fraction ϕ of salt (K_2SO_4) obtained from D_{splay} diffusivities according to the first step of the procedure (see the text). Triangles denote the shear viscosity η measured in this work, as a function of the molar fraction of salt. (b) Two versions of the one elastic constant approximation. Squares denote fixed value for all ϕ (step 1) and triangles denote $K(\phi)$ obtained after identifying $\eta_{\text{splay}} \equiv \eta$ (step 2). (c) Rotational viscosity coefficient versus ϕ. Squares denote $\widetilde{\gamma}_1$ of step 1 and triangles γ_1 of step 2.

initial decrease with increasing ϕ before reaching practically the same values as η. As that initial decrease is a quite odd behavior, we now point out that a much more reasonable hypothesis is to assume that the true η_{splay} is to be identified with the shear viscosity η at each ϕ value. Therefore, according to this view, we should attribute the initial decrease of $\widetilde{\eta}_{\text{splay}}$ rather to an initial increase of the elastic constant $K(\phi)$. That is, in this second step we are going to adopt a ϕ-dependent one-elastic-constant approximation. For instance, for the Nd4a sample we identify $\eta_{\text{splay}} \equiv \eta = 0.204$ Pa s, which implies $K(\phi = 0.25\ \text{mol\%}) = D_{\text{splay}}\eta_{\text{splay}} = 19 \times 10^{-12}\ \text{m}^2/\text{s}\ 0.204\ \text{Pa s} = 3.88 \times 10^{-12}$ N. The same procedure applied to all samples yielded the $K(\phi)$ values listed in Table III [see Fig. 8(b)].

Both hypotheses (steps 1 and 2) comprise some distortions, e.g., the $K(0)$ value for Nd3 is too low. Nevertheless, the step-2 procedure seems to give more consistent results for three reasons. First, it avoids that behavior of η_{splay} that decreases for increasing ϕ, which is physically difficult to explain. Second, $K(\phi)$ first increases with the salt concentration before reaching a saturation plateau [see Fig. 8(b)]. There are theoretical reasons to support such a behavior, as we shall briefly discuss below. Third, the step-2 value of the rotational viscosity γ_1 for the ternary sample (much less than the $\widetilde{\gamma}_1$ of the step-1 hypothesis) agrees quite well with a direct measurement by Kim [29] ($\sim$0.7 Pa s) in the same lyotropic system.

Now turning to the second reason, by considering the IBM model it is possible to qualitatively discuss the role of the salt in the nematic micellar arrangement. In the lyotropic nematic mixtures investigated, micelles present locally an orthorhombic symmetry and are piled up in a pseudolamellar structure [3,30]. Orientational fluctuations of correlation volumes degenerate the symmetry axis perpendicular to the biggest micellar surface and the macroscopic-uniaxial discotic symmetry arises. The salt added to the original ternary mixture dissociates into ions, which are located in the aqueous region of the sample, between the micelles. The increase of the shear viscosity η and rotational (or twist) viscosity γ_1 of the mixtures for increasing salt content may indicate an increase of the dimensions of the micelles [31] and/or an augmentation of the steric micelle-to-micelle interaction (this is due to the decrease of the Debye length and the consequent decrease of the intermicellar distance [32]). The ions from the salt may act like a bridge between neighboring micelles, increasing their electrostatic interaction and hydrogen bonds.

Further studies are necessary to clarify the hypothetical connection between an increase of the salt concentration and an increase of the micellar size. Perhaps a useful hint here results from noticing that the behavior of $K(\phi)$ of Fig. 8(b) bears a resemblance to a theoretical prediction [33] (see the inset of Fig. 1 therein) based on the special case of a pure Nehring-Saupe interaction [33] (see references therein).

V. CONCLUSION

We have investigated the behavior resulting from the addition of salt in a ternary lyotropic mixture presenting the discotic nematic phase, combining DLS and (shear) viscosity measurements. The splay diffusivity initially increases with the increase of the salt concentration and seems to reach an asymptotic behavior. In contrast, the twist diffusivity decreases as the salt concentration increases. In order to estimate the behavior of the corresponding viscosities, we have introduced hypotheses in a two-step approach, regarding the elastic constants. The resulting viscosity estimates yielded a η_{splay} strongly dependent on each hypothesis made. In contrast, the rotational (twist) viscosity coefficient γ_1 showed to be much less sensitive to such hypothetical considerations [see Fig. 8(c)]. Similarly, the backflow term increases as the salt concentration increases, until reaching values about one order of magnitude bigger than that of the ternary mixture (salt-free sample). A possible origin for these behaviors of the viscosity and backflow terms could be attributed to the electrostatic and hydrogen bond interaction between neighboring micelles due to the presence of dissociated ions. Our results show that salt influences both DLS and viscosity measurements, which opens possibilities of controlling the properties of lyotropic liquid crystals.

ACKNOWLEDGMENTS

It is a pleasure to thank Professor I. M. N. de Oliveira for helpful discussions, D. Reis for assistance with the liquid crystal mixture preparations, and A. R. Leite for technical support. We wish to thank Coordenação de Aperfeiçoamento de Pessoal de Nível Superior, CNPq, FAPESP, INCT-FCx, NAP-FCx, and The Scientific and Technological Research Council of Turkey (TÜBİTAK) for financial support.

[1] P. G. de Gennes and J. Prost, *The Physics of Liquid Crystals*, 2nd ed. (Clarendon, Oxford, 1993).
[2] S. Chandrasekhar, *Liquid Crystals*, 2nd ed. (Cambridge University Press, Cambridge, 1992).
[3] A. M. Figueiredo Neto and S. R. A. Salinas, *The Physics of Lyotropic Liquid Crystals: Phase Transitions and Structural Properties* (Oxford University Press, Oxford, 2005).
[4] M. J. Freiser,Phys. Rev. Lett. **24**, 1041 (1970).
[5] Y. Galerne and J. P. Marcerou, Phys. Rev. Lett. **51**, 2109 (1983).
[6] L. J. Yu and A. Saupe, Phys. Rev. Lett. **45**, 1000 (1980).
[7] P. G. de Gennes and J. Prost, *The Physics of Liquid Crystals* (Ref. [1]), p. 141.
[8] M. B. Lacerda Santos and M. A. Amato, Eur. Phys. J. B **7**, 393 (1999).
[9] G. Durand, L. Leger, F. Rondelez, and M. Veyssie (Orsay Liquid Crystal Group), Phys. Rev. Lett. **22**, 1361 (1969).
[10] P. G. de Gennes and J. Prost, *The Physics of Liquid Crystals* (Ref. [1]), p. 206.
[11] M. B. Lacerda Santos, Y. Galerne, and G. Durand, J. Phys. (Paris) **46**, 933 (1985).
[12] M. Čopič, T. Ovsenik, and M. Zgonik, Liq. Cryst. **2**, 643 (1987).
[13] S. Chandrasekhar, *Liquid Crystals* (Ref. [2]), p. 162.
[14] S. Fraden and R. B. Meyer, Phys. Rev. Lett. **57**, 3122 (1986).
[15] E. Akpinar, D. Reis, and A. M. Figueiredo Neto, Eur. Phys. J. E **35**, 50 (2012).
[16] E. Akpinar, D. Reis, and A. M. Figueiredo Neto, Liq. Cryst. **39**, 881 (2012).
[17] A. M. Figueiredo Neto, L. Liébert, and Y. Galerne, J. Phys. Chem. **89**, 3737 (1985).
[18] T. Kroin and A. M. Figueiredo Neto, Phys. Rev. A **36**, R2987 (1987).
[19] B. J. Berne and R. Pecora, *Dynamic Light Scattering* (Wiley, New York, 1976).
[20] M. B. Lacerda Santos, Y. Galerne, and G. Durand, Phys. Rev. Lett. **53**, 787 (1984).
[21] H. Z. Cummins and H. L. Swinney, in *Progress in Optics*, edited by E. Wolf (North-Holland, Amsterdam, 1970), Vol. VIII.
[22] M. Delaye, Ph.D. thesis, Université Paris–Sud, 1978.
[23] P. G. de Gennes and J. Prost, *The Physics of Liquid Crystals* (Ref. [1]), Chap. 3.
[24] W. Helfrich, J. Chem. Phys. **50**, 100 (1969).
[25] T. Kroin, A. J. Palangana, and A. M. Figueiredo Neto, Phys. Rev. A **39**, 5373 (1989).
[26] T. Haven, D. Armitage, and A. Saupe, J. Chem. Phys. **75**, 352 (1981).
[27] M. Stefanov and A. Saupe, Mol. Cryst. Liq. Cryst. **108**, 309 (1984).
[28] M. B. Lacerda Santos and G. Durand, J. Phys. (Paris) **47**, 529 (1986).
[29] Du-Rim Kim, J. Kor. Phys. Soc. **35**, 345 (1999).
[30] A. M. Figueiredo Neto, Y. Galerne, A. M. Levelut, and L. Liebert, J. Phys. Lett. **46**, 499 (1985).
[31] A. Saupe, S. Y. Xu, S. Plumley, Y. K. Zhu, and P. Photinos, Physica A **174**, 195 (1991).
[32] H. S. Park, S. W. Kang, L. Tortora, Y. Nastishin, D. Finotello, S. Kumar, and O. D. Lavrentovich, J. Phys. Chem. B **112**, 16307 (2008).
[33] P. A. de Castro, A. J. Palangana, and L. R. Evangelista, Phys. Rev. E **60**, 6195 (1999).